PNAS
www.pnas.org

Supplementary Information for

High resolution neutron crystallography visualizes an OH-bound resting state of a copper-containing nitrite reductase

Yohta Fukuda, Yu Hirano, Katsuhiro Kusaka, Tsuyoshi Inoue, Taro Tamada

Tsuyoshi Inoue, Taro Tamada
Email: t_inoue@phs.osaka-u.ac.jp (TI); tamada.taro@qst.go.jp (TT)

This PDF file includes:

www.pnas.org/cgi/doi/10.1073/pnas.1918125117

1. Supplementary Results and Discussion

Network of weak hydrogen bonds around T1Cu

The neutron scattering length maps revealed that the first and second coordination spheres of the T1Cu site has a precise hydrogen bond network maintained by standard and weak hydrogen bonds such as CH-O, CH-π, and NH-π hydrogen bonds (*SI Appendix*, Fig S12). Two His ligands to T1Cu, His95 and His143, were protonated at their N^{ε} atoms. His143 is a solvent-exposed ligand, which formed a hydrogen bond with a nearby water molecule. The coordination bond between the N^{δ} atom of His143 and T1Cu was slightly deviated from the imidazole plane. This unusual conformation of His143 seemed to be stabilized by weak interactions with surrounding residues. His143 formed a CH-O hydrogen bond through its C^{δ} and C^{ε} atoms with the carbonyl O atoms of Pro139 and Pro94, respectively. Moreover, the imidazole ring of His143 was sandwiched by Trp63 and Thr137 through the T-shaped π–π and CH-π interactions, respectively. Trp63 may have a role to stabilize the conformation of His143 and is highly conserved among class II CuNIRs (*SI Appendix*, Fig S13). The indole ring of Trp63 formed an NH-π bond with the side chain of Asn146. His95 formed a hydrogen bond with Asp90, which was connected to N-terminal His21. His21 had an indirect interaction with Trp63 through a water molecule as was reported in other *Geobacillus* CuNIR [1]. A CH-O hydrogen bond was found between the C^{δ} atom of His95 and the side chain O atom of Asn88 that also formed a standard hydrogen bond with the main chain amide group of Asp90. The S^{δ} atom of Met148 that coordinated to T1Cu might have a CH-S interaction with the H atom on the C^{β} atom of Trp63 because the distance of CH-S was short (3.0 Å) and a lone pair of the S^{δ} atom presumably directed to the $C^{\beta}H$ atom of Trp63. Two H atoms on the C^{γ} atom of Met148 formed CH-O hydrogen bonds with the carbonyl O atoms of His143 and Trp63, respectively. The conformations of Met ligand vary from CuNIR to CuNIR [2]. Met148 of *Gt*NIR shows a *gauche* conformation that is less stable than the *anti* one found in other CuNIRs such as *Ax*NIR. Our neutron structure indicates that finely tuned weak hydrogen bond networks can stabilize the *gauche* conformation in *Gt*NIR.

2. Materials and Methods

2.1. Expression and purification of *Gt*NIR.

A pET22b plasmid containing *Gt*NIR gene was transformed into *E. coli* BL21(DE3) strain. Expression of the protein was induced by 1 mM IPTG at 20 °C for 18 h. The collected cells were sonicated in buffer A (20 mM Tris-HCl, pH 8.0) and incubated at 70 °C for 120 min. The sample was centrifuged, and 10 mM $CuSO_4$ was added to the supernatant until the color of the solution turned into deep green. The resulting solution was loaded onto a HiLoad 16/60 Superdex 200 column (GE Healthcare). The fractions containing *Gt*NIR were collected and ammonium sulfate was added up to 40% w/v. After incubation at 4 °C for 30 min, the solution was centrifuged and the supernatant was applied onto a HiTrap Phenyl HP column (GE Healthcare). The protein was eluted with a linear gradient of ammonium sulfate, dialyzed against buffer A, and purified with a HiTrap Q HP column using sodium chloride. The fractions containing *Gt*NIR were then loaded onto a HiLoad 16/60 Superdex 200 column equilibrated by buffer A. The peak fractions were collected and concentrated to 90 mg/ml.

2.2. Preparing large crystal of *Gt*NIR.

A high-quality large *Gt*NIR crystal was prepared by a combination of micro- and macro-seeding methods. First, crystals were obtained at 20 °C by the hanging-drop vapor-diffusion method with a 1:1 mixture of the purified protein solution (30 ~ 45 mg/ml) and a reservoir solution containing 0.1 M acetate buffer pH 4.6, 5.0% (w/v) PEG 4000, and 75 mM $CuSO_4$. Obtained crystals were shattered in a drop by a needle. The resulting solution was 10 times diluted by the reservoir solution to make a seed solution. Streak microseeding crystallization was performed at 20 °C by the hanging-drop vapor-diffusion method. We dipped a single hair obtained from one of the authors (a 31-years-old male of *Homo sapiens*) into the seed solution and then run it through the drop of the mixture of a purified protein solution (30 mg/ml; 1.5 µL) and a reservoir solution (0.1 M acetate buffer pH 4.6, 5.5% (w/v) PEG 4000, and 75 mM $CuSO_4$; 1.5 µL) on a siliconized cover glass plate. The cover glass was put on a 0.5 mL sample cups (Sanplatec) containing 400 µL reservoir solution. At this microseeding crystallization step, high-quality small single crystals could be obtained within a day.

Macroseeding crystallization was performed at 20 °C by the floating-drop vapor-diffusion method as described below. The purified protein solution (30 mg/ml; 75 µL) was mixed with a reservoir solution (0.1 M acetate buffer pH 4.6, 5.5% (w/v) PEG 4000, and 50 mM $CuSO_4$; 75 µL) and transferred to an inner dent of a snap cap of a Falcon 14 mL polypropylene round-bottom tube (Corning), which was half-filled with fluorinert (Hampton research) to prevent grown crystals from sticking to the bottom. The outer moat of the snap cap was filled with the reservoir solution. The snap cap was sealed by a 22 mm × 0.22 mm siliconized circle cover slide (Hampton research) and left at 20 °C for 2 days to progress vapor diffusion. A small parallelogram crystal obtained from a microseeding drop was washed several times by the reservoir solution without $CuSO_4$ and transferred to the crystallization set-up in the snap cap with a LithoLoop (Protein Wave).

After we obtained a large-volume crystal, we gradually increased the concentration of D_2O and cryo-protectant (2-methyl-2,4-pentanediol: MPD) in the reservoir by changing the reservoir solutions. The pH was also gradually and slightly changed to pH 4.9 (pD 5.3). At this step, $CuSO_4$ was not included in the used solution. The final reservoir solution contained D_2O, 0.1 M monodeuterated acetate buffer pD 5.3, 5.5% (w/v) PEG 3350, and 30% (v/v) perdeuterated MPD. The crystal was kept in the deuterated solution for 1 week. Because some small crystals were fused during crystal growth, we separated them with a microknife MK-100 (SOSHO).

2.3. Neutron and X-ray diffraction data collection.

A large-volume crystal with an apparent size of 3.4 mm^3 (the actual size may be half or one-third of this) was harvested by a 2 × 3 mm LithoLoop attached on a B3 magnetic goniometer

base (MiTeGen) and flash-cooled in a nitrogen-gas stream at 100 K on a goniometer head at a beamline BL03 iBIX in the Materials and Life Sciences Experimental Facility (MLF) of the Japan Proton Accelerator Research Complex (J-PARC; Tokai, Japan). Time-of-flight (TOF) neutron diffraction data were collected by using thirty wavelength-shifting fiber-based scintillator neutron detectors with an area of 133 × 133 mm^2 [3]. A total of 40 data sets were collected using a wavelength of 2.15-4.89 Å with a sample-to-detector distance of 490 mm. The exposure time for each data set was 6.9 h at 500 kW. This large crystal was also used for cryogenic X-ray diffraction data collection at a beamline AR-NE3A of Photon Factory Advanced Ring (PF-AR; Tsukuba, Japan). Diffraction images were collected at 100 K using a Pilatus 2M-F detector (DECTRIS) with a sample-to-detector distance of 92 mm. The oscillation angle per image was set to 0.1 °. The exposure time per image was set to 0.1 sec. A total of 3600 diffraction images were collected by using a helical scan method to reduce radiation damages.

2.4. Structural determination and refinement.

The TOF neutron data were integrated by a profile fitting method with *STARGazer* [4, 5] and then merged and scaled by *SCALA* [6]. The X-ray diffraction data were processed and scaled by using *XDS* [7] and *AIMLESS* [6], respectively. Molecular replacement phase determination was performed by *MOLREP* [8] with a *Gt*NIR structure (PDB code ID: 4YSO) as a search model. The joint refinement was performed with both the neutron and X-ray diffraction data using *phenix.refine* implemented in *PHENIX* [9]. Five percent of the data were selected by PHENIX for cross-validation. Manual model building was performed using *COOT* [10], through which positions of H (D) atoms and H^+ (D^+) on amino acid residues and orientation of water molecules were manually modeled consulting both the neutron scattering length density and electron density calculated before including hydrogen/deuterium. The temperature factors for all atoms and occupancies for hydrogen/deuterium atoms and residues having dual conformations were also refined. The final model quality was checked by *MolProbity* [11]. The coordinate file and the structure factor file are deposited in the Protein Data Bank (PDB code ID: 6L46). The raw data collected in this study are available at the Integrated Resource for Reproducibility in Macromolecular Crystallography (https://proteindiffraction.org).

3. SI Table

Table S1 | Data collection and refinement statistics

	Neutron	X-ray
Data collection		
Beamline	J-PARC MLF BL03 iBIX	Photon Factory AR-NE3A
Wavelength (Å)	4.89-2.15	1.0000
Space group	*R*3 (*H*3)	
Unit cell *a*, *b*, *c* (Å)	114.2, 114.2, 83.69 (*H*3)	
Resolution range (Å)	17.38-1.50 (1.59-1.50)	42.58-1.03 (1.05-1.03)
R_{merge} (%)	23.0 (60.8)	6.5 (64.1)
$R_{p.i.m.}$ (%)	9.7 (28.5)	2.1 (25.3)
Completeness (%)	99.7 (99.7)	99.9 (98.7)
Total reflections	425,961 (50,384)	1,923,181 (70,086)
Unique reflections	64,997 (9,495)	201,251 (9,887)
$\langle I/\sigma(I)\rangle$	9.5 (2.2)	21.2 (3.5)
$CC_{1/2}$	(0.782)	(0.907)
Redundancy	6.6 (5.3)	9.6 (7.1)
NX Joint Refinement		
Resolution (Å)	17.0-1.50 (1.54-1.50)	34.1-1.30 (1.33-1.30)
R_{work} (%)/ R_{free} (%)	14.2/15.8 (19.0/22.2)	9.62/11.1 (9.49/13.5)
No. of protein atoms	4,952	
No. of ligand atoms/ions	28	
No. of D_2O	458 (including O and OD types)	
Average *B* (Å^2)		
All	15.5	
Protein atoms	12.4	
D_2O	31.8	
Other atoms	21.8	
Ramachandran plot (%)		
Favored	97.3	
Allowed	2.7	
Outliers	0	
PDB code ID	6L46	

4. SI Figures

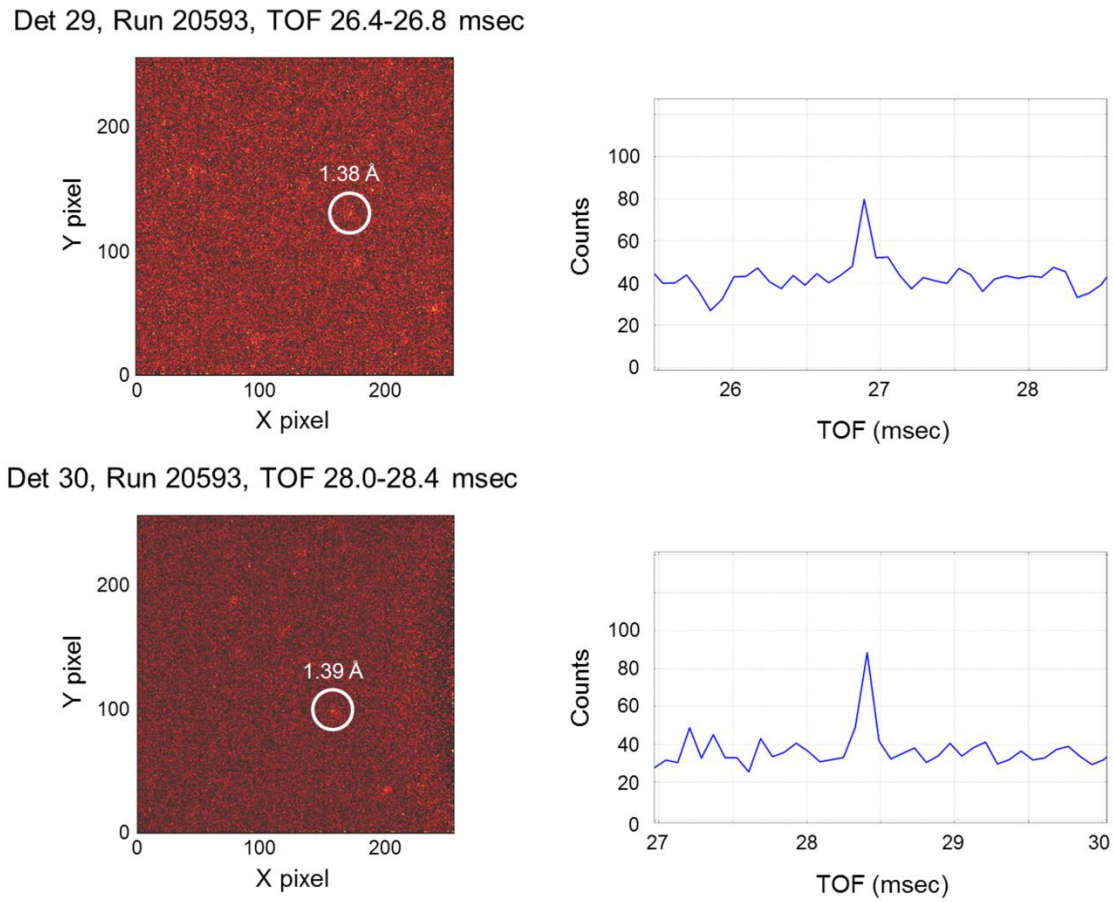

Fig. S1. Selected diffraction spots beyond 1.4 Å resolution. Diffraction images generated by *STARGazer* (left) and their count profiles against TOF (right).

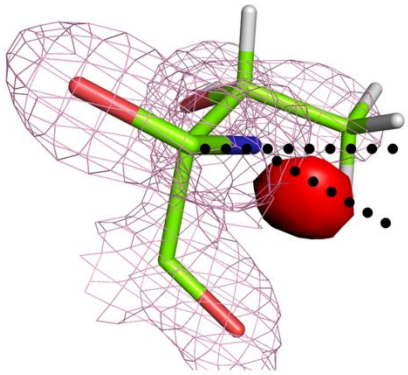

Fig. S2. The distorted peptide bond and the deviated position of the amide H atom of Thr293. Sigma-A-weighted $2F_o–F_c$ (2.0 σ) and $F_o–F_c$ (-3.5 σ) neutron maps are shown by pink mesh and red surface representations, respectively.

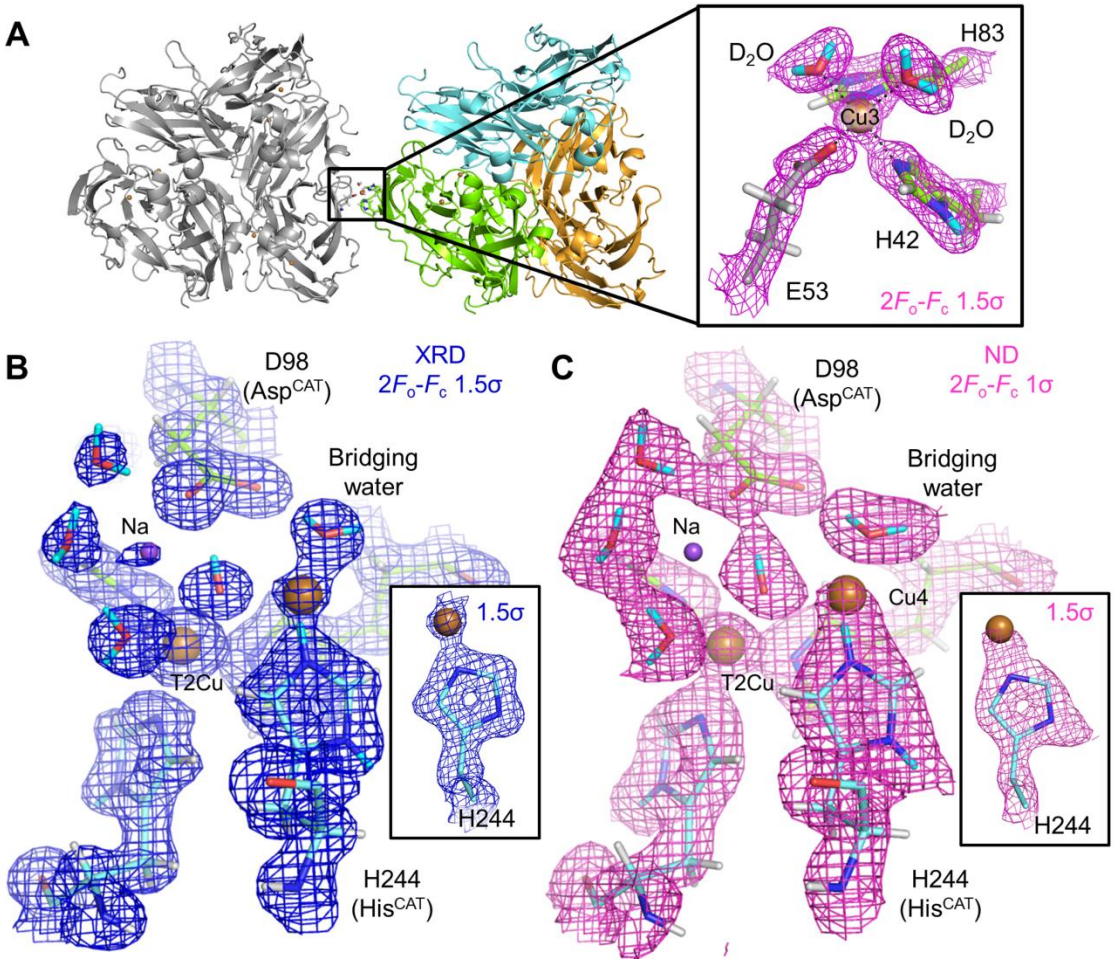

Fig. S3. Artificial copper and sodium sites observed by XRD. (A) The Cu3 site positioned between two trimeric *Gt*NIR molecules. The sigma-A-weighted F_o–F_c neutron map is illustrated by magenta meshes. (B) The sigma-A-weighted $2F_o$–F_c electron density map around the T2Cu site. (C) The sigma-A-weighted $2F_o$–F_c neutron map around the T2Cu site. The Na and Cu atoms are drawn by purple and brown spheres, respectively. Coordination bonds are shown by dotted black lines. D atoms are colored by cyan.

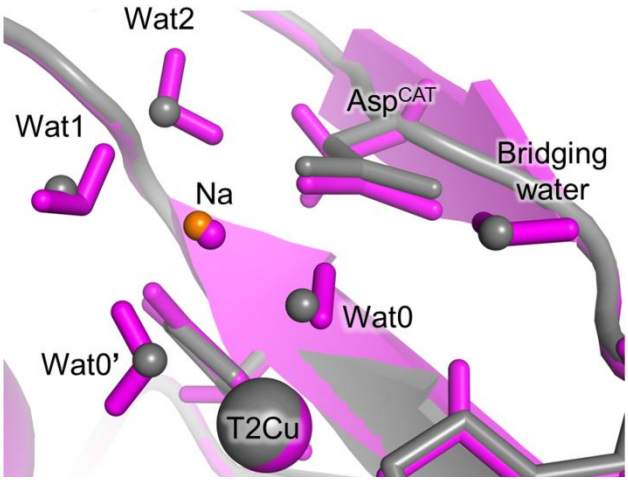

Fig. S4. Comparison of the positions of water molecules between ND and SFX structures. The ND structure is depicted by magenta cartoon, sticks, and a sphere. The SFX structure is illustrated by grey cartoon, sticks, and spheres. The Na ion in the SFX structure is shown by a small orange sphere.

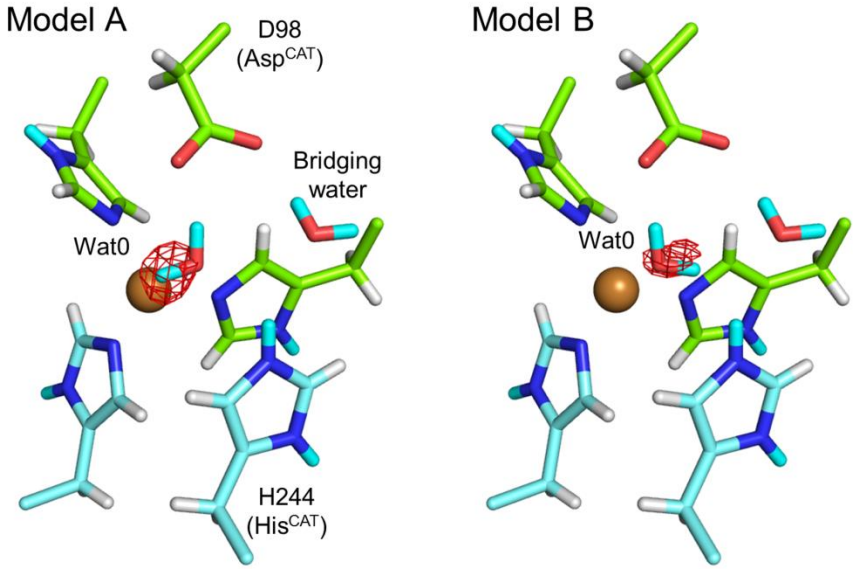

Fig. S5. D_2O molecules modeled at the Wat0 site. The sigma-A-weighted F_o–F_c neutron map contoured at -4.0 σ are illustrated by red meshes.

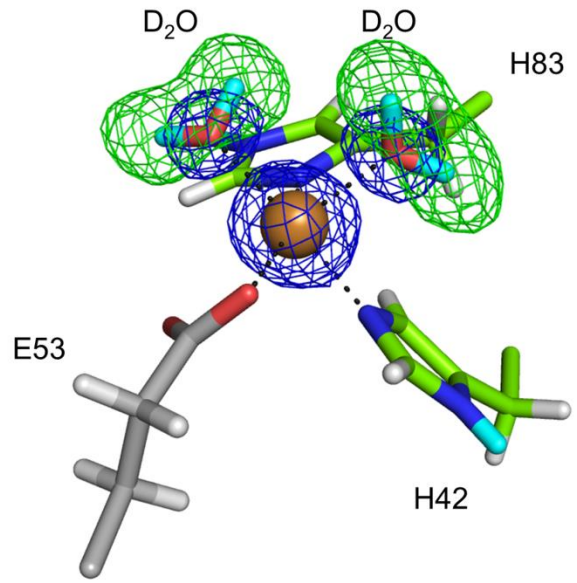

Fig. S6. D_2O molecules on Cu3. The sigma-A-weighted $2F_o–F_c$ electron density map (2.5 σ) and sigma-A-weighted $F_o–F_c$ neutron map (+3.5 σ) are illustrated by blue and green meshes, respectively.

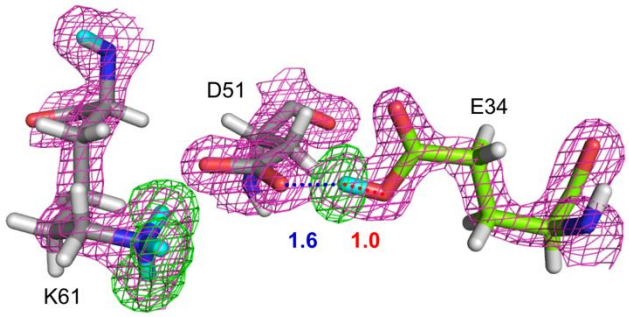

Fig. S7. Deuterated Glu34. The sigma-A-weighted $2F_o–F_c$ (2.0 σ) and $F_o–F_c$ (+4.0 σ) neutron maps are illustrated by magenta and green meshes, respectively. Distances from O atoms to the D atom are shown in Å unit.

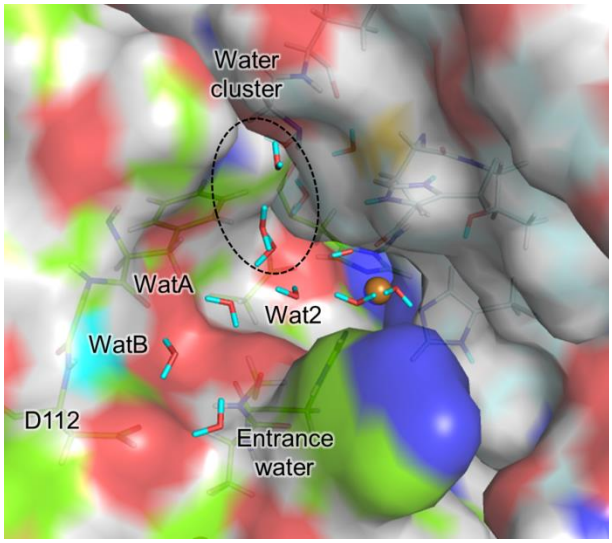

Fig. S8. Water molecules in the MPC shown with the protein surface. Water molecules are represented by sticks. The T2Cu atom is shown by a brown sphere.

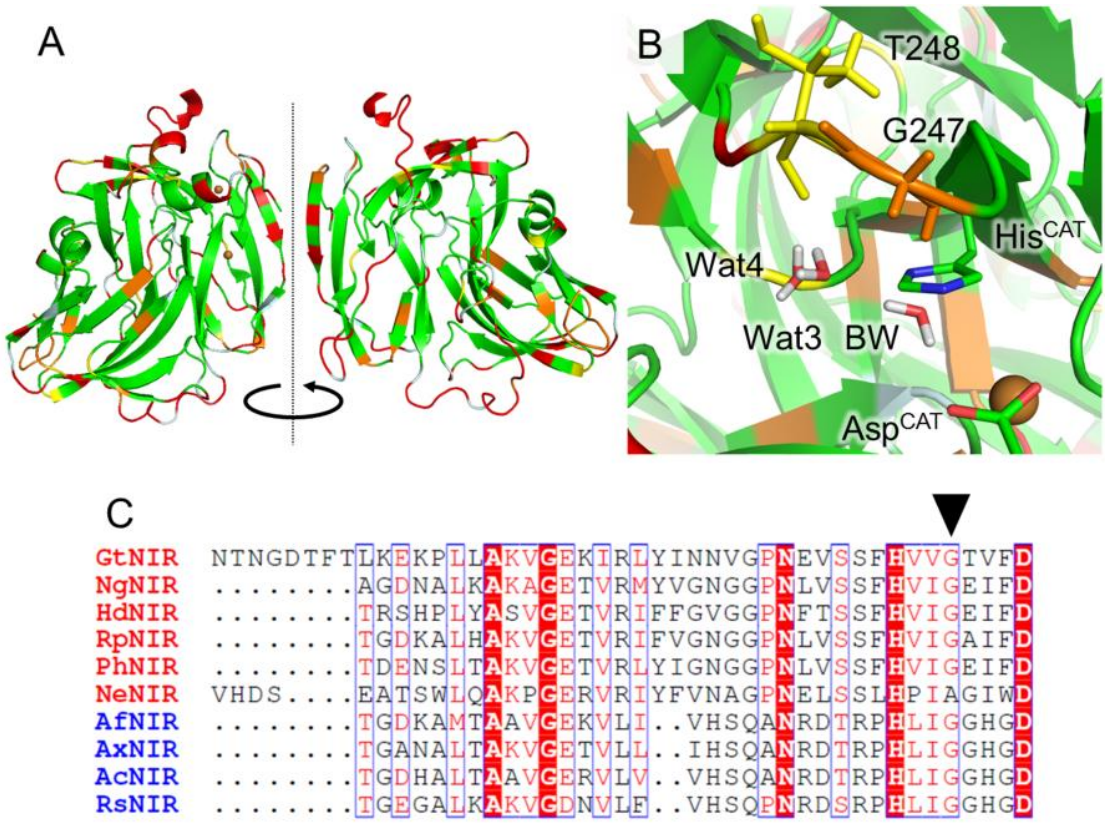

Fig. S9. H-D exchange. (A) The monomeric unit of *Gt*NIR colored according to the deuterium occupancies of backbone amides. Green, negligible occupancy (0–0.15); yellow, low occupancy (0.15–0.3); orange, moderate occupancy (0.3–0.7); red, high occupancy (0.7–1.0). (B) A close-up view around the T2Cu site. (C) Sequence alignment of CuNIRs. The position of conserved Gly is indicated by a black arrow head. Blue and red entry names indicate class I and II CuNIRs, respectively. Ng: *Neisseria gonorrhoeae*; Hd: *Hyphomicrobium denitrificans*; Rp: *Ralstonia pickettii*; Ph: *Pseudoalteromonas haloplanktis*; Ne: *Nitrosomonas europaea*; Af: *Alcaligenes faecalis*; Ax: *Achromobacter xylosoxidans*; Ac: *Achromobacter cycloclastes*; Rs: *Rhodobacter sphaeroides*.

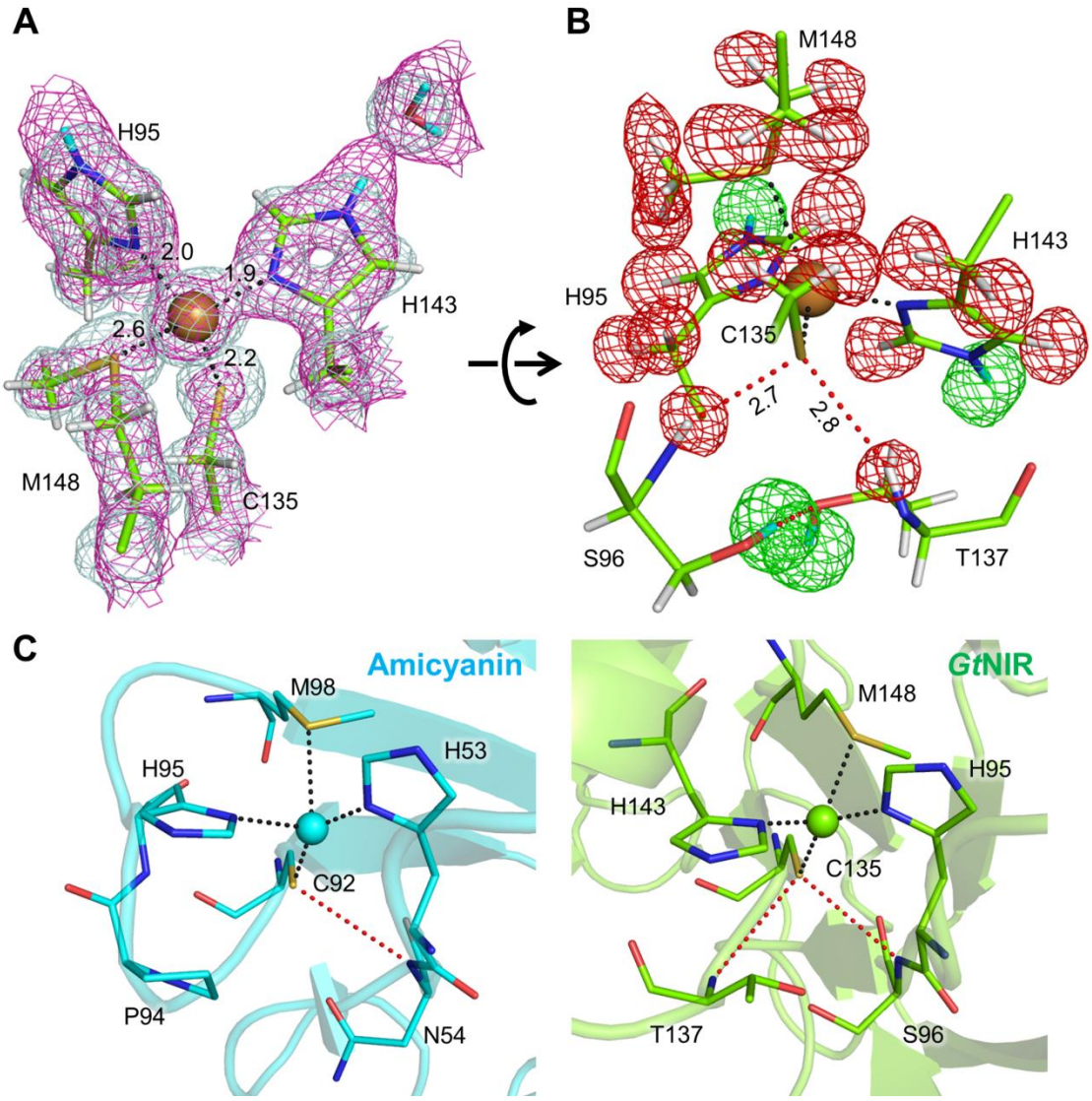

Fig. S10. The structure of the T1Cu site. (A) The coordination structure of the T1Cu site. The sigma-A-weighted $2F_o–F_c$ electron density (1.5 σ) and neutron (1.0 σ) maps are illustrated by sky-blue and magenta meshes, respectively. (B) Positions of H and D atoms. The positive (+3.5 σ) and negative (-3.5 σ) sigma-A-weighted $F_o–F_c$ neutron maps are shown by green and red meshes, respectively. (C) Comparison of NH-S hydrogen bond environments between amicyanin (PDB code ID: 3L45) and *Gt*NIR. Coordination bonds are depicted by dotted black lines and their distances are shown in Å unit. NH-S hydrogen bonds are shown by dotted red lines and their distances are represented by Å unit.

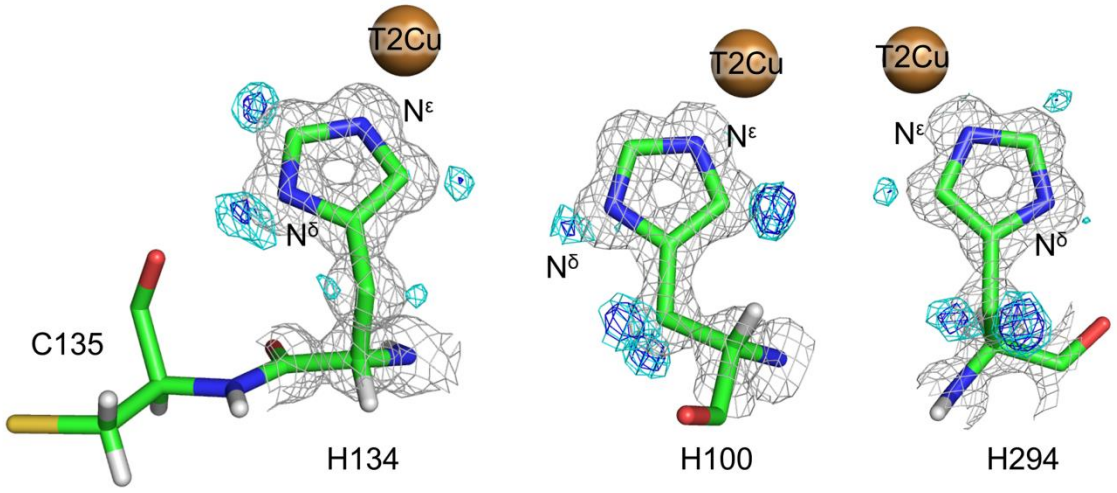

Fig. S11. Electron density of H/D atoms on T2Cu ligand residues. The sigma-A-weighted $2F_o–F_c$ electron density maps (1.5 σ) are illustrated by grey meshes. The sigma-A-weighted H/D omit $F_o–F_c$ electron density maps contoured at +3.0 and +2.3 σ are shown by blue and cyan meshes, respectively. These maps were calculated by using X-ray data up to a resolution of 1.03 Å. This figure shows that the N^{δ} atom of His134 is protonated, and proves that atomic resolution X-ray crystallography is not enough to visualize H/D atoms.

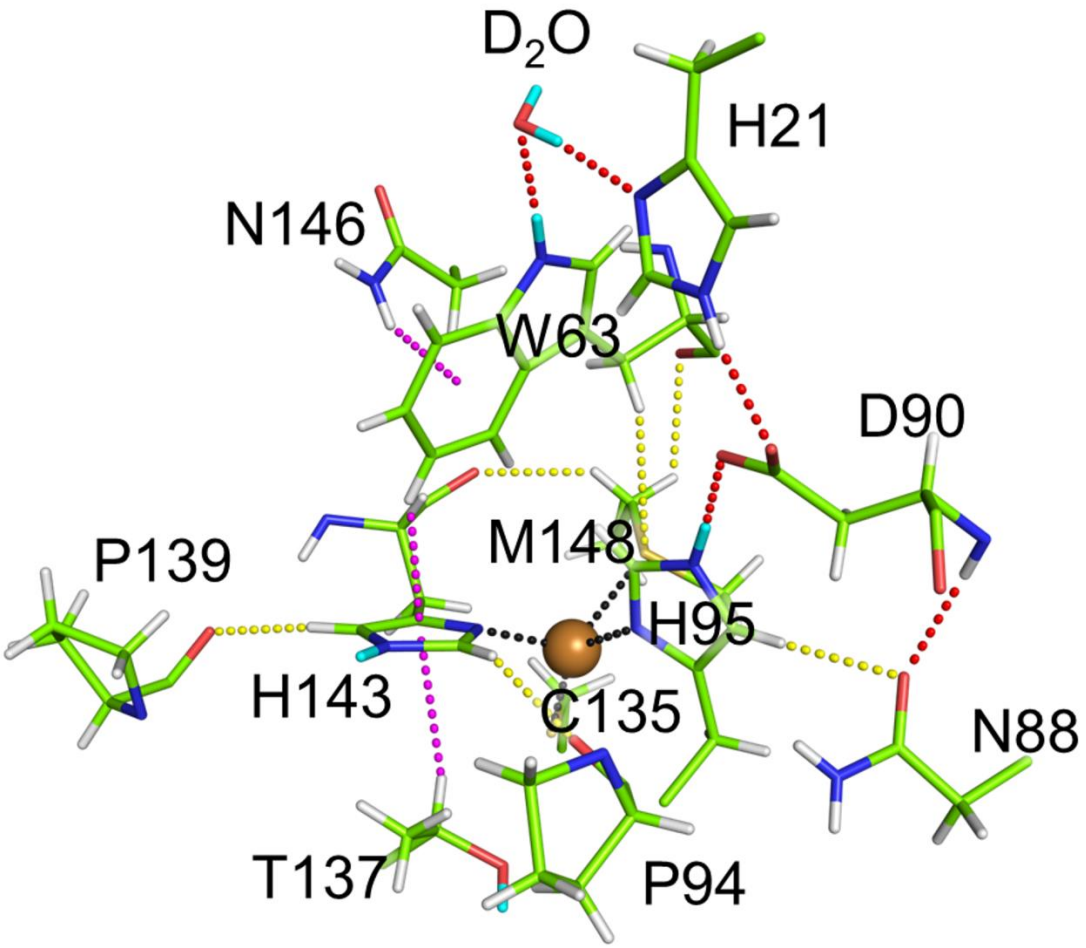

Fig. S12. Weak hydrogen bond interactions around the T1Cu site. CH-O and CH-S hydrogen bonds are shown by dotted yellow lines. NH-π and CH-π interactions are shown by dotted magenta lines. Coordination bonds and standard hydrogen bonds are shown by dotted black and red lines, respectively. D and H atoms are colored by cyan and white, respectively. T1Cu is shown by a brown sphere.

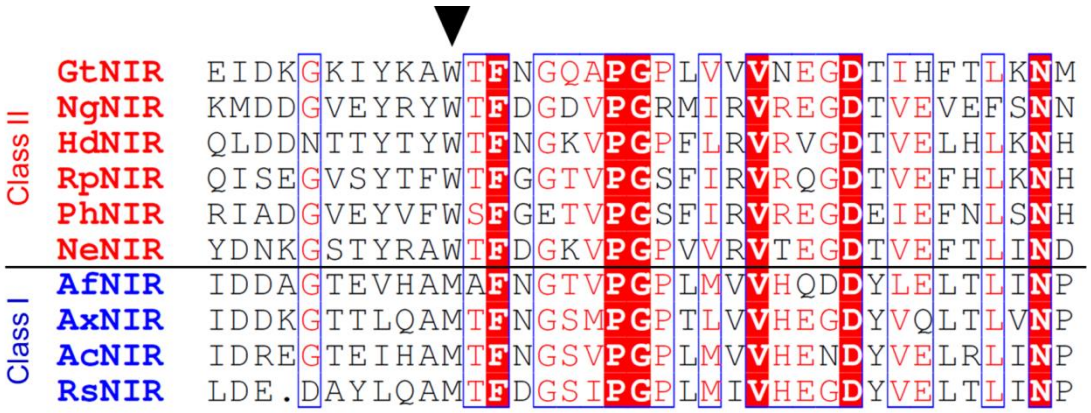

Fig. S13. Sequence alignment of CuNIRs. Residues conserved among all CuNIRs are shown by white characters with red backgrounds. Residues having similar properties are shown by red characters. The position of tryptophan conserved in class II CuNIRs are indicated by a black arrow head. Ng: *Neisseria gonorrhoeae*; Hd: *Hyphomicrobium denitrificans*; Rp: *Ralstonia pickettii*; Ph: *Pseudoalteromonas haloplanktis*; Ne: *Nitrosomonas europaea*; Af: *Alcaligenes faecalis*; Ax: *Achromobacter xylosoxidans*; Ac: *Achromobacter cycloclastes*; Rs: *Rhodobacter sphaeroides*.

5. SI References.

1. Fukuda, Y., Koteishi, H., Yoneda, R., Tamada, T., Takami, H., Inoue, T. & Nojiri, M. Structural and functional characterization of the *Geobacillus* copper nitrite reductase: involvement of the unique N-terminal region in the interprotein electron transfer with its redox partner, *Biochimica et Biophysica Acta*. **1837**, 396-405. (2014)
2. Inoue, T., Gotowda, M., Deligeer, Kataoka, K., Yamaguchi, K., Suzuki, S., Watanabe, H., Gohow, M. & Kai, Y. Type 1 Cu Structure of Blue Nitrite Reductase from *Alcaligenes xylosoxidans* GIFU 1051 at 2.05 Å Resolution: Comparison of Blue and Green Nitrite Reductases, *J Biochem*. **124**, 876-879. (1998)
3. Hosoya, T., Nakamura, T., Katagiri, M., Birumachi, A., Ebine, M. & Soyama, K. Development of a new detector and DAQ systems for iBIX, *Nuclear Instruments and Methods in Physics Research Section A: Accelerators, Spectrometers, Detectors and Associated Equipment*. **600**, 217-219. (2009)
4. Ohhara, T., Kusaka, K., Hosoya, T., Kurihara, K., Tomoyori, K., Niimura, N., Tanaka, I., Suzuki, J., Nakatani, T., Otomo, T., Matsuoka, S., Tomita, K., Nishimaki, Y., Ajima, T. & Ryufuku, S. Development of data processing software for a new TOF single crystal neutron diffractometer at J-PARC, *Nuclear Instruments and Methods in Physics Research Section A: Accelerators, Spectrometers, Detectors and Associated Equipment*. **600**, 195-197. (2009)
5. Yano, N., Yamada, T., Hosoya, T., Ohhara, T., Tanaka, I., Niimura, N. & Kusaka, K. Status of the neutron time-of-flight single-crystal diffraction data-processing software STARGazer, *Acta crystallographica D*. **74**, 1041-1052. (2018)
6. Evans, P. R. An introduction to data reduction: space-group determination, scaling and intensity statistics, *Acta crystallographica D*. **67**, 282-292. (2011)
7. Kabsch, W. Xds, *Acta crystallographica D*. **66**, 125-132. (2010)
8. Vagin, A. & Teplyakov, A. Molecular replacement with MOLREP, *Acta crystallographica D*. **66**, 22-25. (2010)
9. Adams, P. D., Afonine, P. V., Bunkoczi, G., Chen, V. B., Davis, I. W., Echols, N., Headd, J. J., Hung, L. W., Kapral, G. J., Grosse-Kunstleve, R. W., McCoy, A. J., Moriarty, N. W., Oeffner, R., Read, R. J., Richardson, D. C., Richardson, J. S., Terwilliger, T. C. & Zwart, P. H. PHENIX: a comprehensive Python-based system for macromolecular structure solution, *Acta crystallographica D*. **66**, 213-21. (2010)
10. Emsley, P., Lohkamp, B., Scott, W. G. & Cowtan, K. Features and development of Coot, *Acta crystallographica D*. **66**, 486-501. (2010)
11. Chen, V. B., Arendall, W. B., 3rd, Headd, J. J., Keedy, D. A., Immormino, R. M., Kapral, G. J., Murray, L. W., Richardson, J. S. & Richardson, D. C. MolProbity: all-atom structure validation for macromolecular crystallography, *Acta crystallographica D*. **66**, 12-21. (2010)